Enhancement of Magnetic Fluid Multimode Interference Filter-Based on No-Core Fiber in the Fourth Self-Imaging

Batool M.Saloom [1], Anwaar A. Al-Dergazly [2*], Haider Al-Juboori[3]

Authors affiliations:
1) Laser and Optoelectronic Engineering Department, Al-Naharain University, Baghdad, Iraq.
Batool.m.saloom@ced.nahrainuniv.edu.iq

2*) Laser and Optoelectronic Engineering Department, Al-Naharain University, Baghdad, Iraq.
anwar.a.al_dergazly@nahrainuniv.edu.iq

3) South East Technological University, Faculty of Engineering, Department of Electronics Eng. & Com., Carlow, Ireland.
haider.aljuboori@setu.ie

Paper History:

Received: 25th Aug. 2024

Revised: 20th Oct. 2024

Accepted: 23rd Dec. 2024

Abstract

Cascade single mode fiber—no core fiber—single mode fiber (SNS) filters are experimentally demonstrated and theoretically investigated by COMSOL6.1. Multiphysics. These devices' simplicity, compactness, affordability, all-fiber design, low transmission loss, and ability to continuously adjust the laser wavelength at a particular spectral range contribute to their dependability. The operation's basis is multimode interference (MMI) and self-image phenomena. A SNS filter based on an optimized 4th self-imaging condition for different no-core fiber (NCF) dimensions was theoretically optimized at λpeak/dip=1550 nm, then a magnatic tunable filter encircled by ferrofluid was experimentally investigated at 4th self-imaging. The theoretical results are indicate that reducing the NCF diameter can enhance the filter's tunability. At 4th self-image, the maximum tunability of DNCF = 40 μm and LNCF = 0.6 cm is about 260 nm from 1429 nm to 1689 nm. The experimental results show that the tunability of a filter based on a magnetic field reaches about 5 nm (1550.9 nm -1555.9 nm). LNCF=58.5 mm and NCF diameter 125 μm. device has applications in fiber laser technology, spectroscopy, and optical communication.

Keywords: Multimode Interferometry (MMI) , Ferrofluid , Magnetic Field Filter, Self-Imaging , Optimization , Tunability.

تحسين مرشح التداخل متعدد الأوضاع للسوائل المغناطيسية القائم على الألياف غير الأساسية في التصوير الذاتي الرابع

بتول محمود سلوم، انوار الدركزلي، حيدر الجبوري

الخلاصة:

تم إثبات مرشحات الألياف أحادية الوضع المتتالية - بدون ألياف أساسية - الألياف أحادية الوضع (SNS) تجريبياً وتم التحقيق فيها نظرياً بواسطة COMSOL6.1. Multiphysics. إن بساطة هذه الأجهزة واكتنازها وقدرتها على تحمل التكاليف وتصميمها بالكامل من الألياف وانخفاض خسارة الإرسال والقدرة على ضبط طول موجة الليزر باستمرار عند نطاق طيفي معين تساهم في موثوقيتها. أساس العملية هو التداخل متعدد الأوضاع (MMI) وظاهرة الصورة الذاتية. تم تحسين مرشح SNS المستند إلى حالة تصوير ذاتي رابعة مُحسَّنة لأبعاد مختلفة للألياف بدون نواة (NCF) نظريًا عند λpeak/dip=1550nm، ثم تم التحقيق تجريبياً في مرشح قابل للضبط المغناطيسي محاط بسائل مغناطيسي عند التصوير الذاتي الرابع. تشير النتائج النظرية إلى أن تقليل قطر NCF يمكن أن يعزز قابلية ضبط المرشح. في الصورة الذاتية الرابعة، يكون الحد الأقصى لضبط DNCF = 40 ميكرومتر و LNCF = 0.6 سم حوالي 260 نانومتر من 1429 إلى 1689 نانومتر. تظهر النتائج التجريبية أن ضبط المرشح القائم على المجال المغناطيسي يصل إلى حوالي 5 نانومتر (1550.9 نانومتر _1555.9 نانومتر). LNCF = 58.5 م وقطر NCF 125 ميكرومتر. للجهاز تطبيقات في تكنولوجيا الليزر الليفي، والتحليل الطيفي، والاتصالات البصرية.

1. Introduction

Optical fibers, with their large bandwidth and low power losses, contributed to the quick development of optical communications. .[1] Optical fiber-based devices with more flexible features were created, such as tunable fiber lenses[2] and bandpass filters[3]Nowadays, the usage of fiber optics MMI devices is common, owing to their ease of fabrication: in its most basic form, it consists of sandwiching a multimode fiber (MMF) between two single-mode fibers (SMFs). All of the mentioned ones allow simple, robust, and highly repeatable fiber-based devices. Furthermore, the performance of MMI devices, notably their spectrum response, is determined by both geometric and optical characteristics. These characteristics provide several degrees of freedom for manipulating and controlling MMI devices, making them particularly adaptable in applications. The bulk of MMI operations have been associated with combined the field of optics including MMI. Optical couplers [4][5], MMI splitters for sensors [6]and MMI switching [7], [8], Fiber-based MMI system research is still in its early stages, with just a few devices previously shown thus far. A key feature of fiber-based MMI device is their reliance on the wavelength dependency demonstrated by the self-image phenomenon. As a result, the fiber-based MMI functions as a band-pass filter, making it suitable for a variety of applications. They've been employed as movement sensor [9]as band-pass filters [3]and as sources of single-transverse-mode lasers from multiple modes of active fibers [10]. With the advent of nanotechnology, a new class of smart nanomaterials appears as an useful foundation for novel optoelectronic devices. Ferrofluids (FFs) or magnetic fluids, which are stable colloidal solutions which includes surfactant-coated magnetic nanoparticles distributed in an appropriate liquid, have the magnetism of magnetic nanoparticles as well as the fluidity of liquid materials [11][12].External magnetic fields can adjust FFs' unique characteristics, including optical anisotropy and birefringence, the Faraday effect, tunable refractive index, and field-dependent transmission. Because of their excellent magneto-optical abilities, FFs have been utilized to create novel photonic devices such as optical switches[13],optical modulators[14],tunable optical filters[15],optical fiber gratings[16],and sensors[17][18]. Fiber optic filters based on single-mode—no-core—single-mode (SNS) structures have various benefits, such as low cost and simple fabrication, compared to other optical fiber filter .In this paper, we optimized the tunability of the MMI filter for different NCF dimensions for 4th self-image theoretically via COMSOL Multiphysics software and investigated experimentally the magneto-optical filter-based NCF.

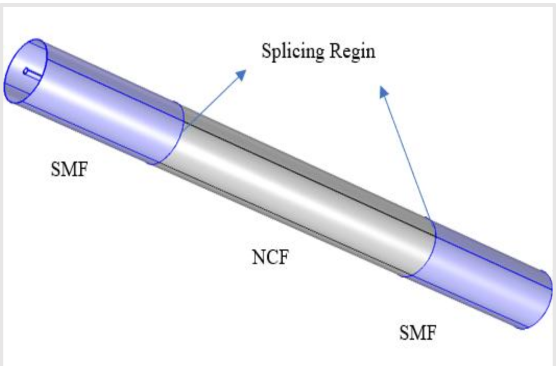

Figure (1): Single mode -No-Core-Single mode fiber Filter

2. Self-Imaging in SNS Structure

The single mode input from SMF stimulates multiple linearly polarized LP_{0m} higher order fiber modes in the MMF because of their circular symmetry and an absence of lateral offset between the axis of the SMFs and MMF following fusion splicing. The modulated transmission optical response at the end of the MMF is directed back to the output SMF as a result of interference between the many modes traveling with different phases and velocity along the MMF. According to the SNS filter structure, the transmittance is given as[19].

$$T = 10\log_{10}\left[\frac{|\sum_{m=1}^{M} C_M^2\, exp(-\gamma_m L) exp(-i\beta_m L)|2}{\sum_{m=1}^{M} C_M^2}\right] \quad \textbf{(1)}$$

Where T is the transmittance , L is fiber length, C_M is the excitation coefficient of m^{th} excited mode (m = 1,2,3,...,n), γ_m is the evanescent field absorption coe1fficient, and β_m is the propagation constant of the m^{th} order mode. When various modes are activated inside the fiber's multi-mode segment, the input field is repeated at regular intervals throughout its length, a phenomenon referred to as self-imaging. The length of the MMF section required to generate the periodic image of the input field is stated as [20]

$$L \cong p\left(\frac{n_{MMF} D^2{}_{MMF}}{\lambda_0}\right) \quad where\ p = 0,1,2,3,4, \ldots (2)$$

Here, n_{MMF} and $D\ _{MMF}$signify the refractive index (RI) and the diameter of the MMF core where ($D\ _{MMF}$ ≫ λ_0, free space wavelength). In particular, every fourth image (p=4N, with N = 1,2,3,..) reproduces the input field's exact profile, including a narrow transmitted peak/dip at an identified central wavelength, including a narrow transmitted dip at a specific central wavelength.Fig. 1 show the SNS filter stuctue.Equation (2) confirm that the 4th self-imaging length is greater for bigger diameter fibers 2 ($L \propto D^2{}_{MMF}$)for a certain wavelength or shorter wavelengths for a specific fiber diameter ($L \propto \frac{1}{\lambda_0}$) and vice versa. This study takes use of the fourth self-imaging condition's limited spectral response.

Magnetic fluid/ferrofluid is a low-cost material having a variety of physical, thermal, and tunable magneto-optical characteristics, including refractive index (RI), absorption coefficient, and birefringence[21] [22][23][24]. Whenever a magnetic field is applied over a specific critical field intensity, scattered magnetic nanoparticles begin to combine and form magnetic chain/column structures along the magnetic field direction until saturate [25][26]Propagation and chain formation are affected by the temperature (T) and magnetic field (H), resulting in a tunable absorption coefficient and refractive index (RI) of the MF material. The refractive index (n_{MF}) of the MF is defined as [27]

$$n_{MF}\ \ (H,T) = (n_s - n_0)L(H,T) + n_O,$$
$$For H > H_C \qquad \ldots..(3)$$

Where L (H, T) = [Coth (α$\frac{H-H_C}{T}$) − ($\frac{T}{\alpha(H-H_C)}$)] is Langevin function. Here, H and T are applied magnetic field (Gauss) and temperature (Kelvin) of MF, H_c is the critical field strength (which is the minimum field required to align the magnetic domains along the direction of field overcoming the fluid thermo-dynamics of the MF, below which there is no column formation and n_o change in RI), n_s and n_o are the RIs at saturation field ($H = H_{sat}$) and at field below critical field ($H < H_c$) respectively, α is fitting parameter. Besides magnitudes of H and T, the n_{MF} change also depends on the relative direction of magnetic field with respect to light propagation direction (k), concentration of the magnetic particles in the colloidal solution, type of carrier liquid and the light-MF interaction length[25] [27].

The n_{MF} rises with the strength of the magnetic field above $\boldsymbol{Tc}$ if the magnetic field is parallel to the light transmission direction ($i.e.\ \boldsymbol{T} \parallel k$), and reduces with field intensity if the H-field direction is perpendicular to the propagation direction k ($i.e.\ \boldsymbol{T} \perp k$) [25] [28]. Furthermore, when $H \parallel k$, the magnetic field has a wider refractive index modulation varied than when $\boldsymbol{T} \perp k$. This n_{MF} reliance on relative orientation between H & k is connected with the so-called magnetoelectric directing effect when electric susceptibility χ varies as a result of magnetic field $\chi = \chi(\boldsymbol{T})$ [29]and is expressed as:

$$n_{MF} = \sqrt{\varepsilon} = \sqrt{1 + \chi\,(\mathrm{H})} \qquad \ldots\ldots(4)$$

The microstructural modifications of MF into column formation, which modify the effective concentration, absorption, and scattering cross-sections in the presence of an increasing external magnetic field, are responsible for the tunable transmittance of MF[30] [31]. At zero H-fields, the MF with uniformly dispersed Fe_3O_4 is basically a liquid phase that is semi-transparent to light; however, as the H-field intensity increases, Fe_3O_4 gradually evolve into column-like microstructures, resulting in a liquid-solid phases.

The measurement approach used here is the relative loss of intensity with respect to the 4th-self imaging wavelength dip in an SNS filter using magnetic fluid forming the cladding of the NCF fiber.

3. Results and Discussion

In this section we will discuss the theoretical results.

3.1 Self-Imaging Condition Optimization in SNS Filter

The optimization of the SNS structure for the fourth self-imaging condition is based on both the NCF length and diameter optimization, allowing for greater tunbility to transmission loss Fig.2 show 4th self-imaging condition D_{NCF} =40 μm, L=0.6 cm, λ = 1550nm . The NCF length mostly determines the central wavelength of the interference peak/dip.The refractive index of the cladding/ medium selected close the RI of the NCF core (n_{core}=1.444) lets more evanescent field access to the medium around it, thus offering higher contact with the material used for thus tunbility, yet being too near and above the RI of the core produces total intensity loss because the fiber waveguide just stimulates the cladding modes and not the core modes.

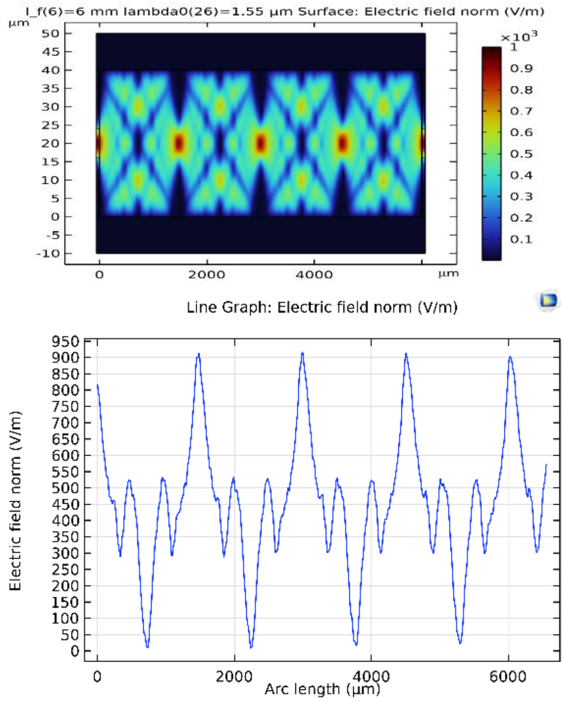

Figure (2): 4th self-imaging condition based on COMSOL simulation with NCF length optimized for MMI fiber structure showing interference E-field patterns and E-field amplitude along the propagation lengths: **(a) & (b)** for for D_NCF =40 μm, L=0.6cm, λ = 1550nm

3.2 Optimization of NCF length for 4th self-imaging

In order to achieve a transmitted intensity dip at a required wavelength,for instance, the 4th self-imaging lengths for 125μm, 80μm, and 60μm diameter fibers with a transmitted dip at 1550 nm are 5.85 cm, 2.4cm and 1.35 cm, consequently [32].The corresponding wavelength shift per cm length ($\Delta\lambda/\Delta L$) on each of these NCF fibers are approximately 26 nm/cm, 63 nm/cm, 114nm/mm and maximum tunability is 260nm/mm as the length deviates ±1mm from the 4th self-imaging length needed for 1550 nm dip (calculated utilizing Eq.2). we examined altering NCF lengths in increments of 0.1 mm and observed the shift of the 4th self-imaging dip wavelength is blue shift when the NCF length increased .We subsequently compared the results of the simulation for the following NCF core fiber length: 5.85 cm (Fig. 3. a & b), 2.4cm (Fig. 3. c & d), 1.35 cm (Fig. 3. e & f) and 0.6 cm (Fig. 3. g &h) optimized for wavelength: 1550 nm. when predicted, the transmitted fourth self-imaging dip (P= 4) red shifts linearly when the NCF length decreases and inversely.

3.2 Experimental setup and result

Figure 4-2 (a) shows the experimental setup for the magnetic field filter. a physical representation of the experimental setup consists of a broad band source (BBS), an optical spectrum analyzer (OSA) (FTB-2-PRO), and a filter based - NCF. To use the SNCS fiber filter, a short length of NCF is sandwiched between two standard SMF-28 fibers, one for lead-in and one for lead-out. For this experiment, the NCF is 125μm.

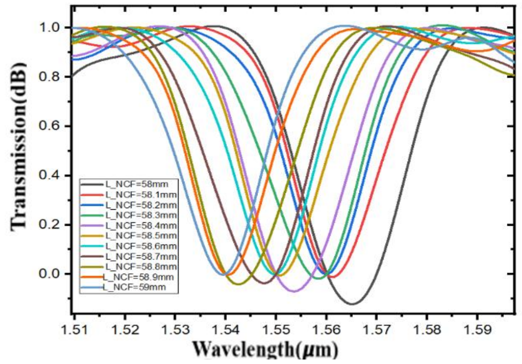

(a)

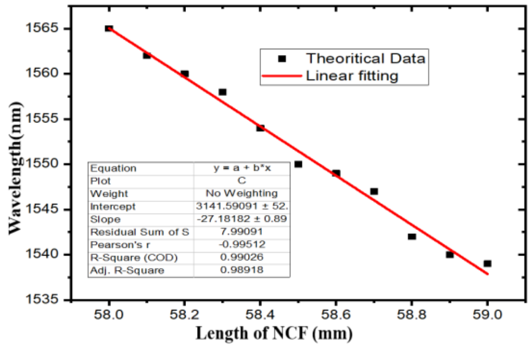

(b)

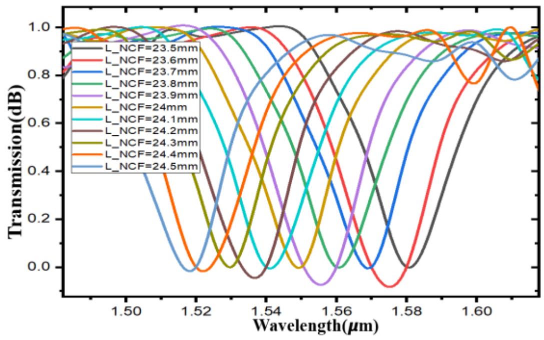

(c)

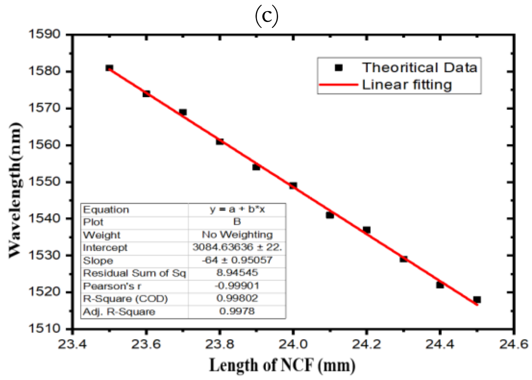

(d)

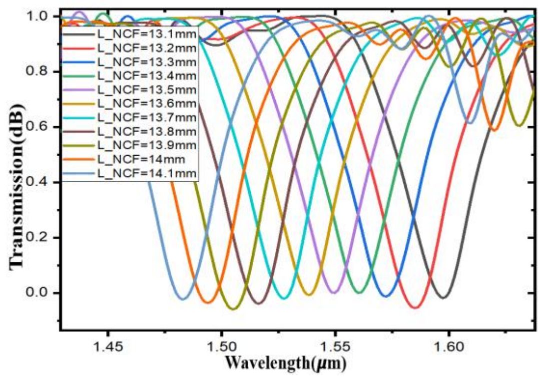

(e)

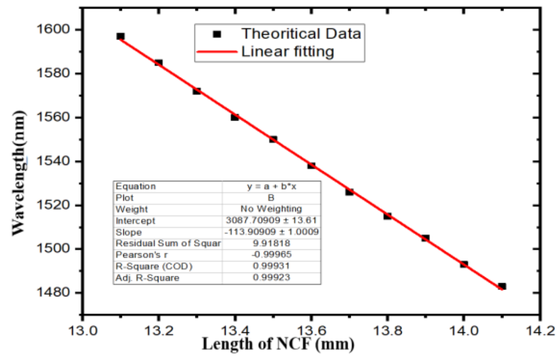

(f)

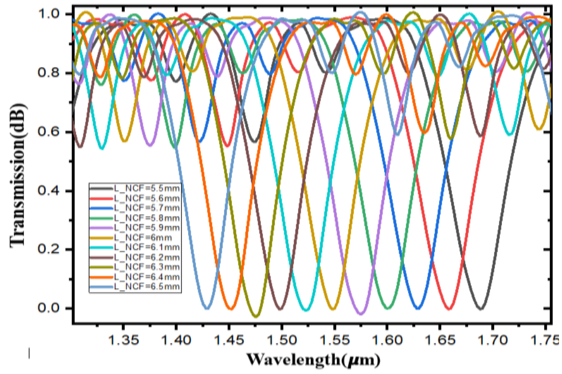

(g)

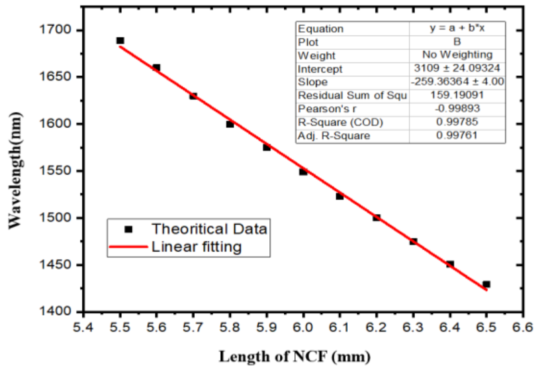

(h)

Figure (3): Transmitted intensity loss of 4th self-imaging peak/dip for various filter with different NCF length (a) SNS filter with (D_{NCF}= 125um, L_{NCF}=58mm -59mm). (c) SNS filter with (D_{NCF}= 60um, L_{NCF}=23.5mm -24.5mm) ,(e) SNS filter with (D_{NCF}= 60um, L_{NCF}=13.1mm -14.1mm) and (g) SNS filter with (D_{NCF}= 40um, L_{NCF}=5.5mm -6.5mm). (b) (d)(f) (h) show the relative linear fitting of the 4th self-imaging dip for four SNS filter.

The experimental work consisted of two essential stages. First, SNS is constructed using a commercial arc fusion splicer (type SWIFT KF4 from ILSINTECH). The splicer was set to automatic mode to reduce splicing losses to the minimum possible. Based on the simulation results, we found that 4thSelf-image It can be achieved at NCF length 58.5 mm and NCF diameter 125um . The operating concept is based on the MMI effect .The SNS structure is formed by splicing a NCF (NCF125) between two SMFs. SMFs have core/cladding dimensions of 8.5 μm and 125 μm, respectively. Before splicing, the protective coating layer was removed with a fiber stripper. Next, the fiber ends were carefully cut. A correct splice requires the cut end-face to be precisely flat and perpendicular to the fiber's axis. Figure 4-1 displays the splicing joint and tapering area, each having splicing losses of less than 0.5 dB. This illustration clearly shows a tapering zone near the splicing junction. Simulation findings indicate that the needed length of NCF is 58.5 mm, ensuring the filter works at 1550 nm and 125 μm NCF diameter.A precise Vernier caliper was used to measure the length of the NCF. Finally, the outside surface of NCF was washed with alcohol and covered with ferrofluid which consist of the carriers are water, and the magnetic particle is Fe_3O_4 with concentrations (φ = 0.5%) .During the testing the SNS filter was securely extended and connected to a glass slide at both ends using joining tape to avoid the effects of fiber bending on its wavelength transmission properties. The purpose of the SMF safety layers was to prevent slide contact. A difference of approximately 85μm proved between the filter and the slide. All experimental measurements were conducted at room temperature.

Table (1): SNS filter based on optimized 4th self-imaging condition for different NCF- Specifications

NCF-Specifications	4th self-Imaging $\lambda_{peak/dip}$ (nm)	Response linearity	Tunability (nm/cm)
D_{NCF}= 125 μm., L_{NCF}= 5.8 cm	1550 nm	R^2 =0.99026	26
D_{NCF} = 80 μm., L_{NCF}= 2.4 cm	1550 nm	R^2 =0.99802	63
D_{NCF}= 60 μm., L_{NCF}= 1.3 cm	1550 nm	R^2 =0.99923	114
D_{NCF}= 40 μm., L_{NCF}= 0.6 cm	1550 nm	R^2 =0.99785	260

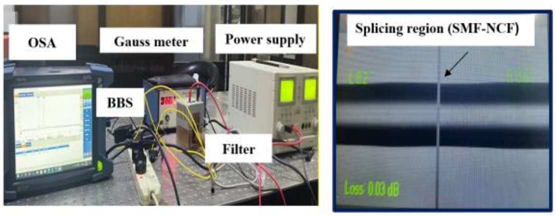

Figure (4): (Left) The experimental setup of cascaded tunable filter, **(Right)** Splicing process of NCF with SMF.

3.3. Tunable Filter Based on Multimode Interference

Figure 4.a, show the variation of intensity dip as a function of magnetic field strength for the NCF length 58.5 mm and NCF diameter 125um. The experimental results show that the tunability of magnetic field measurement reach about 5nm (1550.9 nm _1555.9 nm) From Fig. 4. b, it can be predicted that the intensity dip of output light changes slightly for the magnetic field below 5mT, It is found that the dip intensity of output light is function of the applied magnetic field. the intensity of the output light tends to be constant for the magnetic strength range beyond the saturation magnetization of Fe_3O_4 magnetic nanoparticles which is above 50 mT, is not investigated in this study Similarly, observe the 4th self-imaging peak location as it disappears in the general interference spectra across various wavelengths[2][33]. So, one requires a balance between the intended fourth self-imaging dip wavelength and the RI of the filter.

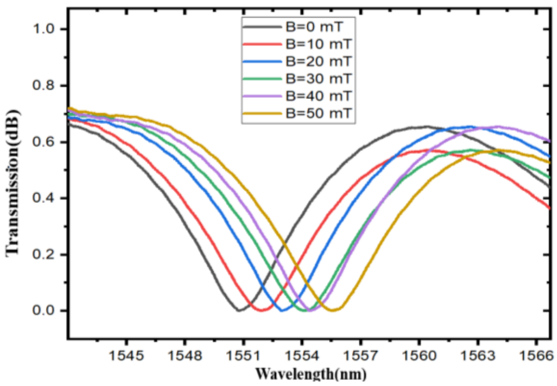

(a)

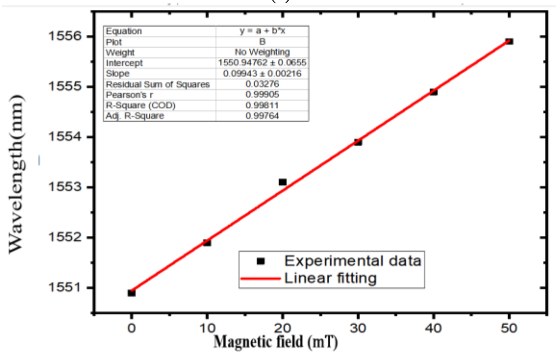

(b)

Figure (4): (a) The transmission of the SNS filter at L_{NCF} =58.5mm and D_{NCF}=125um utilizing Ferrofluid, (b) the dip wavelength shift as a function of the applied magnetic field.

4. Conclusions

A theoretical simulation and experimental investigation have been used to optimize the SNS filter for the optimal spectral condition, namely the fourth self-imaging condition. The center wavelength of the SNS at the 4th self-imaging peak may be precisely adjusted within a few nanometers of the free spectral range. The four SNS filters with four distinct NCF core diameters, optimized for the fourth self-imaging spectral response, produced good response linearity (R-squared value as high as 0.99923). When the RI of the fluid is closer to the NCF core index, it yields maximum tunability. In the magnetic field level below 50 mT,. Further improvement of the filtre performance can be achieved by using magnetic fluid with greater saturation magnetization magnetic nanoparticles and a carrier fluid refractive index that is closer to the NCF core index.

5. References:

[1] A. Castillo-Guzman, J. E. Antonio-Lopez, R. Selvas-Aguilar, D. A. May-Arrioja, J. Estudillo-Ayala, and P. LiKamWa, "Telecomm tunable fiber laser based on multimode interference effect," in Proc. IEEE/LEOS Summer Topical Meetings, 2008, pp. 17–18. doi: 10.1109/LEOSST.2008.4590467.
[2] C. Hong, H.-E. Horng, and S.-Y. Yang, "Tunable refractive index of magnetic fluids and its

applications," Phys. Status Solidi A, vol. 1, no. 7, pp. 1604–1609, 2004. doi: 10.1002/pssc.200304388.
[3] W. S. Mohammed, P. W. E. Smith, and X. Gu, "All-fiber multimode interference bandpass filter," Opt. Lett., vol. 31, no. 17, pp. 2547–2549, 2006. doi: 10.1364/OL.31.002547.
[4] L. B. Soldano and E. C. M. Pennings, "Optical multi-mode interference devices based on self-imaging: principles and applications," J. Lightw. Technol., vol. 13, no. 4, pp. 615–627, 1995. doi: 10.1109/50.372474.
[5] L. B. Soldano, F. B. Veerman, M. K. Smit, B. H. Verbeek, A. H. Dubost, and E. C. M. Pennings, "Planar monomode optical couplers based on multimode interference effects," J. Lightw. Technol., vol. 10, no. 12, pp. 1843–1850, 1992. doi: 10.1109/50.202837.
[6] D. A. May-Arrioja, P. LiKamWa, J. J. Sanchez-Mondragon, R. J. Selvas-Aguilar, and I. Torres-Gomez, "A reconfigurable multimode interference splitter for sensing applications," Meas. Sci. Technol., vol. 18, no. 10, p. 3241, 2007. doi: 10.1088/0957-0233/18/10/S29.
[7] M. P. Earnshaw and D. W. E. Allsopp, "Semiconductor space switches based on multimode interference couplers," J. Lightw. Technol., vol. 20, no. 4, p. 643, 2002. doi: 10.1109/50.996585.
[8] D. A. May-Arrioja, N. Bickel, and P. LiKamWa, "Robust 2×2 multimode interference optical switch," Opt. Quantum Electron., vol. 38, pp. 557–566, 2006. doi: 10.1007/s11082-005-4699-y.
[9] A. Mehta, W. S. Mohammed, and E. G. Johnson, "Multimode interference-based fiber-optic displacement sensor," IEEE Photon. Technol. Lett., vol. 15, no. 8, pp. 1129–1131, 2003. doi: 10.1109/LPT.2003.815338.
[10] X. Zhu, Y. Chen, H. Zhang, L. Wang, and Q. Yu, "Single-transverse-mode output from a fiber laser based on multimode interference," Opt. Lett., vol. 33, no. 9, pp. 908–910, 2008. doi: 10.1364/OL.33.000908.
[11] S. P. Gubin, Y. A. Koksharov, G. B. Khomutov, and G. Y. Yurkov, "Magnetic nanoparticles: preparation, structure and properties," Russ. Chem. Rev., vol. 74, no. 6, p. 489, 2005. doi: 10.1070/RC2005v074n06ABEH000897.
[12] L. Luo, S. Pu, S. Dong, and J. Tang, "Fiber-optic magnetic field sensor using magnetic fluid as the cladding," Sens. Actuators A Phys., vol. 236, pp. 67–72, 2015. doi: 10.1016/j.sna.2015.10.034.
[13] H.-E. Horng, J.-J. Chieh, Y. H. Chao, S.-Y. Yang, C.-Y. Hong, and H.-C. Yang, "Tunable optical switch using magnetic fluids," Appl. Phys. Lett., vol. 85, no. 23, pp. 5592–5594, 2004. doi: 10.1063/1.1833564.
[14] H.-E. Horng, J.-J. Chieh, Y. H. Chao, S.-Y. Yang, C.-Y. Hong, and H.-C. Yang, "Designing optical-fiber modulators by using magnetic fluids," Opt. Lett., vol. 30, no. 5, pp. 543–545, 2005. doi: 10.1364/OL.30.000543.
[15] T. Liu, X. Chen, Z. Di, J. Zhang, X. Li, and J. Chen, "Tunable magneto-optical wavelength filter of long-period fiber grating with magnetic fluids," Appl. Phys. Lett., vol. 91, no. 12, 2007. doi: 10.1063/1.2787970.
[16] A. Candiani, W. Margulis, C. Sterner, M. Konstantaki, and S. Pissadakis, "Phase-shifted Bragg microstructured optical fiber gratings utilizing infiltrated ferrofluids," Opt. Lett., vol. 36, no. 13, pp. 2548–2550, 2011. doi: 10.1364/OL.36.002548.
[17] Y. Zhao, X. Liu, R.-Q. Lv, Y.-N. Zhang, and Q. Wang, "Review on optical fiber sensors based on the refractive index tunability of ferrofluid," J. Lightw. Technol., vol. 35, no. 16, pp. 3406–3412, 2016. doi: 10.1109/JLT.2016.2573288.
[18] N. Cennamo, F. Arcadio, V. Marletta, S. Baglio, L. Zeni, and B. Andò, "A magnetic field sensor based on SPR-POF platforms and ferrofluids," IEEE Trans. Instrum. Meas., vol. 70, pp. 1–10, 2020. doi: 10.1109/TIM.2020.3035114.
[19] Y. Qi, L. Ma, Z. Kang, Y. Bai, and S. Jian, "Tunable all fiber multi-wavelength mode-locked laser using polarization controller coiled SMF-GIMF-SMF structure as both saturable absorber and comb filter," Opt. Fiber Technol., vol. 74, p. 103055, 2022. doi: 10.1016/j.yofte.2022.103055.
[20] P. Zhang, T. Wang, W. Ma, K. Dong, and H. Jiang, "Tunable multiwavelength Tm-doped fiber laser based on the multimode interference effect," Appl. Opt., vol. 54, no. 15, pp. 4667–4671, 2015. doi: 10.1364/AO.54.004667.
[21] T. Walbaum and C. Fallnich, "Wavelength tuning of multimode interference bandpass filters by mechanical bending: experiment and theory in comparison," Appl. Phys. B, vol. 108, pp. 117–124, 2012. doi: 10.1007/s00340-012-5084-8.
[22] H. Li, Z. Wang, C. Li, J. Zhang, and S. Xu, "Mode-locked Tm fiber laser using SMF-SIMF-GIMF-SMF fiber structure as a saturable absorber," Opt. Express, vol. 25, no. 22, pp. 26546–26553, 2017. doi: 10.1364/OE.25.026546.
[23] J. Chen, D. N. Wang, and Z. Wang, "Wavelength-switchable multiple type bound solitons in a passively mode-locked Er-doped fiber laser," IEEE Photonics Technol. Lett., vol. 32, no. 22, pp. 1447-1450, 2020. doi: 10.1109/LPT.2020.3031919
[24] L. Ma, Y. Qi, Z. Kang, Y. Bai, and S. Jian, "Tunable fiber laser based on the refractive index characteristic of MMI effects," Opt. Laser Technol., vol. 57, pp. 96–99, 2014. doi: 10.1016/j.optlastec.2013.10.001.
[25] J. Yu, X. Ma, Y. Qi, Z. Kang, and S. Jian, "All-fiber CW optical parametric oscillator tuned from 1642.5 to 1655.4 nm by a low-loss SMS filter," Results Phys., vol. 17, p. 103136, 2020. doi: 10.1016/j.rinp.2020.103136.
[26] J. E. Antonio-Lopez, J. J. Sanchez-Mondragon, P. LiKamWa, and D. A. May-Arrioja, "Wide range optofluidically tunable multimode interference fiber laser," Laser Phys., vol. 24, no. 8, 2014. doi: 10.1088/1054-660X/24/8/085108.
[27] X. Ma, D. Chen, Q. Shi, G. Feng, and J. Yang, "Widely tunable thulium-doped fiber laser based on multimode interference with a large no-core

fiber," J. Lightw. Technol., vol. 32, no. 19, pp. 3234–3238, 2014. doi: 10.1109/JLT.2014.2342251.

[28] A. Castillo-Guzman, J. E. Antonio-Lopez, R. Selvas-Aguilar, D. A. May-Arrioja, J. Estudillo-Ayala, and P. LiKamWa, "Widely tunable erbium-doped fiber laser based on multimode interference effect," Opt. Express, vol. 18, no. 2, pp. 591–597, 2010. doi: 10.1364/OE.18.000591.

[29] G. Yin, S. Lou, P. Hua, X. Wang, and B. Han, "Tunable fiber laser by cascading twin core fiber-based directional couplers," IEEE Photon. Technol. Lett., vol. 26, no. 22, pp. 2279–2282, 2014. doi: 10.1109/LPT.2014.2351808.

[30] G. Yin, S. Lou, X. Wang, and B. Han, "Tunable multi-wavelength erbium-doped fiber laser by cascading a standard Mach-Zehnder interferometer and a twin-core fiber-based filter," Laser Phys. Lett., vol. 10, no. 12, p. 125110, 2013. doi: 10.1088/1612-2011/10/12/125110.

[31] L. Zhang, X. Wang, X. Liu, J. Zheng, and Y. Liu, "Room-temperature power-stabilized narrow-linewidth tunable erbium-doped fiber ring laser based on cascaded Mach-Zehnder interferometers with different free spectral range for strain sensing," J. Lightw. Technol., vol. 38, no. 7, pp. 1966–1974, 2020. doi: 10.1109/JLT.2020.2971666.

[32] X. Fang, Y. Xuan, and Q. Li, "Measurement of the extinction coefficients of magnetic fluids," Nanoscale Res. Lett., vol. 6, pp. 1–5, 2011. doi: 10.1186/1556-276X-6-237.

[33] J. Chen, D. N. Wang, and Z. Wang, "Wavelength-switchable multiple type bound solitons in a passively mode-locked Er-doped fiber laser," IEEE Photon. Technol. Lett., vol. 32, no. 22, pp. 1447–1450, 2020. doi: 10.1109/LPT.2020.3031919.